IEEE Access
Multidisciplinary : Rapid Review : Open Access Journal

Received 20 January 2023, accepted 19 February 2023, date of publication 22 February 2023, date of current version 1 March 2023.

Digital Object Identifier 10.1109/ACCESS.2023.3247738

RESEARCH ARTICLE

Effect of Driver Mass Loading on Bone Conduction Transfer in an Implantable Bone Conduction Transducer

DONG HO SHIN[1], KI WOONG SEONG[2], AND KYU-YUP LEE[3]
[1]Institute of Biomedical Engineering Research, Kyungpook National University, Daegu 41944, Republic of Korea
[2]Department of Biomedical Engineering, Kyungpook National University Hospital, Daegu 41944, Republic of Korea
[3]Department of Otorhinolaryngology-Head and Neck Surgery, School of Medicine, Kyungpook National University, Daegu 41944, Republic of Korea

Corresponding author: Kyu-Yup Lee (drlky@hanmail.net)

This work was supported in part by the Korea Health Technology Research and Development Project through the Korea Health Industry Development Institute (KHIDI), funded by the Ministry of Health and Welfare, Republic of Korea, under Grant HI18C1892; and in part by the National Research Foundation of Korea (NRF) through the Korea Government (MSIP) under Grant NRF-2022R1A2C4001232.

ABSTRACT This paper focuses on transducers, which are the most important components of bone conduction implants. To improve vibration magnitude, we develop a coil vibration transducer in which the driver mass loading is reduced by about 3.25-fold compared to magnet vibration transducers. We use finite element analysis to derive and implement the maximum Lorentz force and frequency characteristics. We compare the effect of driver mass loading on the vibration magnitude to that of an older transducer. The new transducer vibrates about 4.4-fold more strongly. To compare force magnitude between the two transducers, output force is measured using an artificial mastoid. The force imparted by the new transducer is higher than that of the older transducer only below 1.4 kHz, and tends to be lower at high frequencies. Nevertheless, the improved force in the low-frequency region will improve conductive hearing loss.

INDEX TERMS Artificial mastoid, bone conduction implants, finite element analysis, output force level, transducer.

I. INTRODUCTION

More than 5% of the worldwide population requires hearing devices [1]. The prevalence of hearing loss increases with age; over 25% of those aged more than 60 years suffer from hearing loss [2]. The number of people with noise-induced hearing loss is increasing [3]. Hearing devices employ various sound transmission mechanisms [4], [5], [6], [7], [8], [9], [10], [11], [12]; the most popular hearing devices are air conduction hearing aids (ACHAs), middle ear implants (MEIs), and cochlear implants (CIs) [13], [14], [15]. The indications for ACHAs and CIs are mild-to-moderate and profound loss or deafness, respectively [16], [17]. MEIs are used to overcome moderate hearing loss accompanying sensorineural hearing loss [18]. Although ACHAs are preferred, disadvantages include limited output, acoustic feedback, and ear canal occlusion [19].

The associate editor coordinating the review of this manuscript and approving it for publication was Agustin Leobardo Herrera-May.

MEIs accurately reproduce natural sounds; a small device that generates sound vibrations is attached to the ossicles or located in the round window [20], [21], [22]. However, implantation requires surgery [23]. CIs are effective for profound hearing loss. The indications for CI differ significantly from those for hearing aid systems. CIs do not amplify sound, unlike an ACHA or MEI; instead, they transmit sound by electrically stimulating the auditory nerve [24], [25].

Recently, bone conduction implants (BCIs) have emerged as attractive options for people who cannot use conventional hearing aids [26], [27], [28]. A BCI transmits sound (via bone) to the inner ear; a transducer is implanted behind the ear, in the mastoid region [29]. BCIs are mainly used to correct conductive or mixed-type hearing loss; they transmit a maximum of 50–70 dB HL [30]. As the external auditory canal is not manipulated, there is no discomfort or sense of occlusion caused by ear blockage, and no risk to residual hearing [31], [32]. BCIs can be used by patients unsuitable for conventional hearing aids (ACHAs, MEIs) because of ear

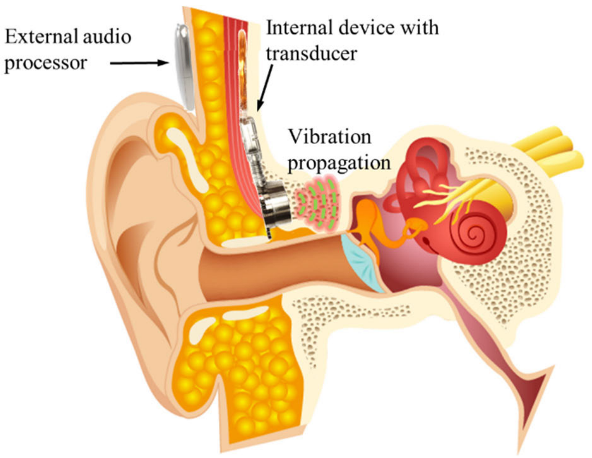

FIGURE 1. Schematic of a bone conduction implant.

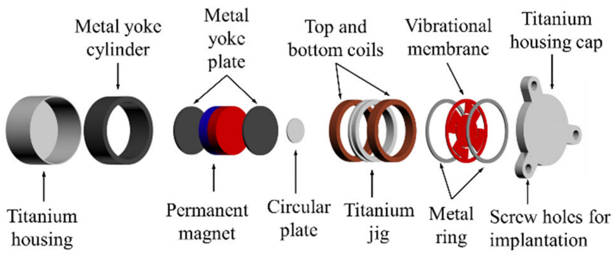

FIGURE 2. Exploded view of the coil vibration transducer.

deformities or infections of the outer or middle ear [33]. However, a BCI must transmit vibrations through the temporal bone; thus, there is a limit to the power of BCIs and they may not be suitable for people with hearing loss > 70 dB [34], [35]. Therefore, a BCI transducer that generates strong vibrations is needed.

To improve vibrational displacement, Shin et al. developed an electromagnetic BCI transducer using a permanent magnet, magnetic yoke, and two coils (top and bottom) wound in opposite directions [36]. Lee et al. miniaturized and optimized the frequency characteristics of the transducer [37]. The mechanical resonance frequency was modified by varying the membrane stiffness and mass of the magnet. The two coils are firmly fixed within a titanium case; when a current flows, a permanent magnet connected to the membrane vibrates via electromagnetic interaction (the Lorentz force) between the coil and magnet. The magnet is heavy compared to the coil. The attenuation of vibrational displacement by mass is greater for magnets than coils. Therefore, to improve the output of the BCI transducer, it is necessary to reduce the attenuation of vibration displacement caused by mass loading. To this end, we developed a BCI transducer in which a coil vibrates, rather than a magnet. The transducer has two coils fixed by a titanium jig, a highly permeable metal yoke, a permanent magnet, a vibrational membrane with a cantilever, a metal ring, a circular plate, and titanium housing; the transducer resembles that of Lee et al [37]. We subjected the vibrational membrane with the cantilever to finite element analysis (FEA) and used the frequency data for fabricating the transducer. To confirm the desired output characteristics, frequency responses were measured using a laser Doppler vibrometer (LDV) and artificial mastoid. Finally, we compared the new transducer with an older model.

II. METHODS

A. STRUCTURE

BCIs have a transducer implanted under the skin of the transmastoid region and an external audio processor that collects sounds (Fig. 1). BCIs transmit vibrations generated by the transducer to the cochlea via bone; the signal does not pass through the external or middle ear. The cochlea converts vibration signals into electrical signals that the cerebrum recognizes as sounds; individuals with hearing impairment are thus able to hear [38]. However, as the vibration is transmitted through bone, some high frequency portion of the signal is lost [39], [40], [41]. Therefore, the transducer output must be high.

A previous study (Lee et al.) miniaturized and optimized the frequency characteristics of the transducer [37]. An effort was made to compensate for the reduction of vibrational force caused by miniaturization using a magnetic yoke fabricated from a highly permeable metal. However, although the location of the resonance frequency and the size may be appropriate for a BCI transducer, the permanent magnet is too small (5 mm in diameter and 4 mm in height) to generate an adequate Lorentz force. This force greatly affects transducer output; the Lee transducer did not adequately compensate for the conductive hearing loss [37]. We improved the output of a BCI transducer using components nearly identical to those of the older transducer (Lee et al.; Fig. 2) [37], thus a titanium housing, a highly permeable metal yoke (the cylinder and plate), a permanent magnet, a circular plate (to secure the space between the membrane and magnet), top (forward-wound) and bottom (reverse-wound) coils, a metal ring, a vibrational membrane with cantilevers, and a titanium housing cap. The difference is that we added a titanium jig to connect the two coils in the floating state. To increase the Lorentz force, the magnet is 10 mm in diameter and 5 mm in height.

Fig. 3 shows cross-sectional views of the older transducer [Fig. 3(a)] and new transducer [Fig. 3(b)]. Both transducers can be viewed as mass-spring-damper systems with mass (m), spring (k), and damping (c) parameters. The solution, X, is the theoretical transducer vibration displacement [42], [43]:

$$m\ddot{x} + c\dot{x} + kx = F_0 sin\omega t \tag{1}$$

$$X = \frac{F_0}{\sqrt{\left(k - m\omega^2\right)^2 + (c\omega)^2}} \tag{2}$$

where m is the mass of the driver (the permanent magnet or coils), k the spring constant of the vibrational membrane, F_0 the electromagnetic force generated by the permanent

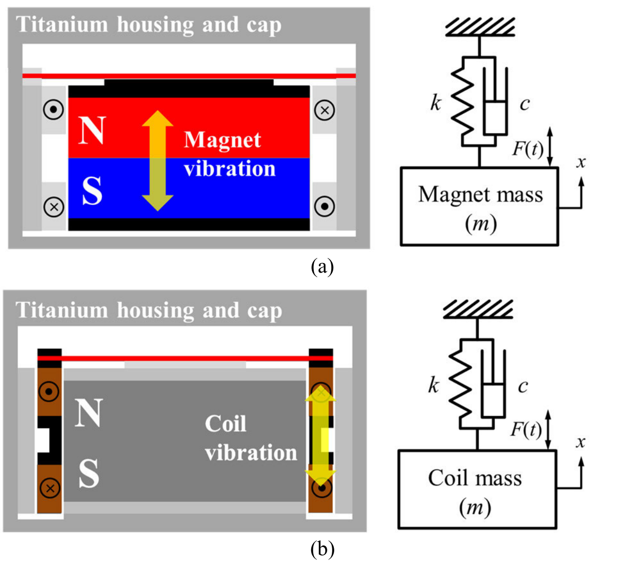

FIGURE 3. Cross-sectional view of the mass-spring-damper system of BCI transducers: (a) magnet vibration transducer and (b) coil vibration transducer.

magnet and coils when current flows, c is viscous damping coefficient, and ω the angular frequency.

As shown in Equation (2), the transducer vibrational displacement is affected by the mass (m); as the driver mass increases, the vibrational displacement decreases. Thus, in the magnet vibration-type transducer [Fig. 3(a)], the use of a heavier magnet than the coil as the driver mass reduces the vibrational displacement compared to that of the coil vibration-type transducer [Fig. 3(b)]. It is essential to minimize the driver mass. Although the theoretical displacement of the coil vibration transducer can be obtained using the above formula, it is very difficult to mathematically derive the magnitude of the electromagnetic force in Equation (1). To predict the electromagnetic (i.e., Lorentz) force generated by interaction between the permanent magnet and the coils, we used software employing the finite element method. The force was mathematically modeled and thus numerically interpretable.

B. ELECTROMAGNETIC ANALYSIS

Both transducers are 15 mm in diameter. However, mounting the feedthrough connector on the titanium housing cap increased the height of the new transducer by 1.5 mm (to 11.5 mm). We used COMSOL Multiphysics (ver. 6.0; COMSOL Inc., Stockholm, Sweden) to derive the maximum Lorentz force of the coil vibration transducer attributable to magnetic flux between the permanent magnet and coils. The magnet was 10 mm in diameter and 5 mm in height. The size of the air gap must be carefully considered when designing a transducer. An air gap of 0.01 mm would be optimal, but it is very difficult to reproducibly ensure such a gap at the laboratory level. Therefore, to ensure reproducibility, the coil was set to have an air gap of 0.1 mm from the permanent magnet and the metal yoke cylinder, respectively. Each coil

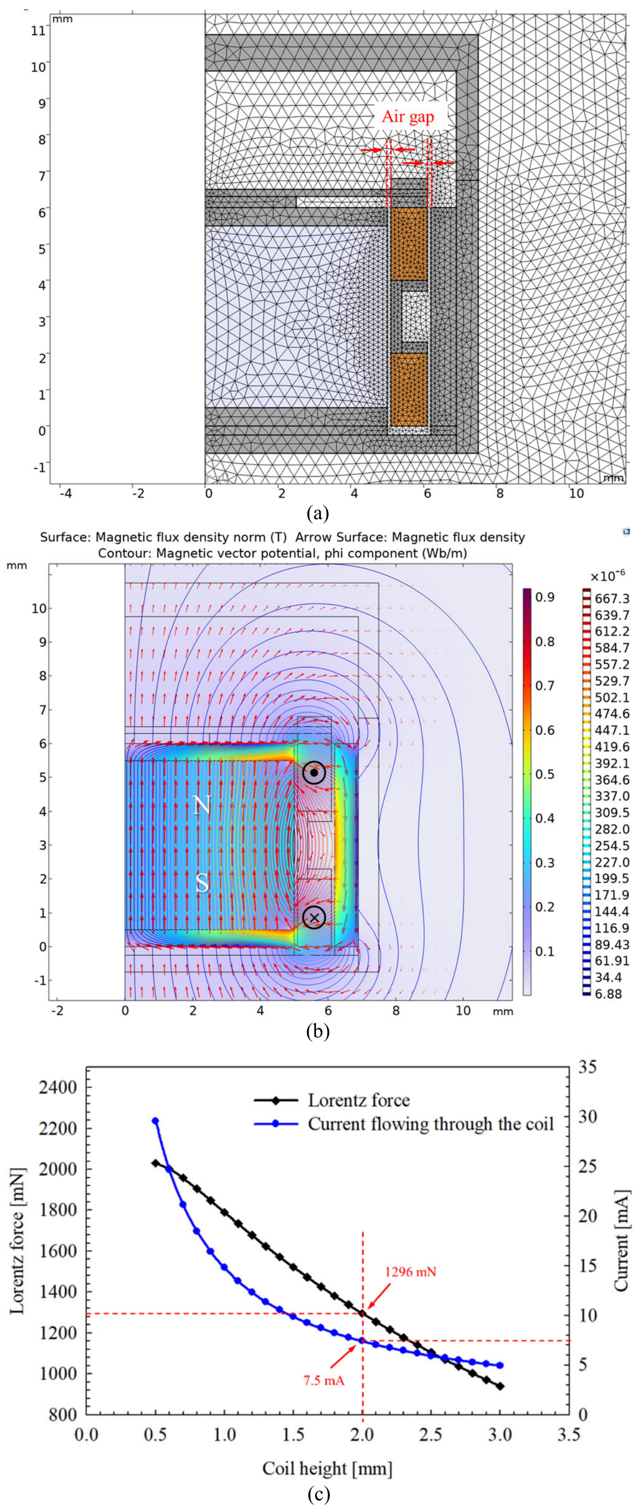

FIGURE 4. (a) Two-dimensional axisymmetric model of the coil vibration-type BCI transducer; (b) magnetic flux density according to the magnetic flux linkage between the permanent magnet and the coil; and, (c) the Lorentz force and current flowing through the coil according to the coil height.

had an outer diameter of 12.2 mm, inner diameter of 10.2 mm, and thickness of 0.059 mm (including the insulation and self-bonding layers). The BCI system under development at Kyungpook National University Hospital (KNUH) uses a 3.7 V_p battery; the maximum voltage and current transmitted from the external to internal device (via an inductive link) are 2.7 V_p and 7.5 mA, respectively. Therefore, during the analysis, the voltage applied to the transducer coil was 2.7 V_p.

The two-dimensional axisymmetric model used for the analysis is shown in Fig. 4(a); all components of the transducer were modeled using the magnetic field routine of the AC/DC module. The surface Gauss of the permanent magnet (NdFeB, grade N38AH) (371 mT) was measured with a tesla meter (TM-801; Kanetec Co. Ltd., Nagano, Japan). Each coil was modeled as a homogeneous multi-turn conductor (wire conductivity = 4.3E7 S/m). To link the magnetic flux generated by the permanent magnet to the magnetic flux of the coil, a highly permeable metal yoke (Mu-metal; relative permeability, 80,000; electrical conductivity, 1.6E6 S/m) was used. The mesh type was free triangular, and the mesh model had 16,173 domain and 849 boundary elements (maximum size, 0.4 mm; minimum size, 0.0008 mm; maximum growth rate, 1.1; curvature factor, 0.2; narrow region resolution, 1). To determine the coil size that generated the maximum Lorentz force, electromagnetic analysis was performed while changing the coil height from 0.5 to 3 mm in 0.1 mm increments. Fig. 4(b) shows the magnetic flux density revealed by the analysis of magnetic flux linkage between the permanent magnet and coil. Fig. 4(c) shows the Lorentz force and current flowing in the coil according to the coil height when 2.7 V_p was applied. As the current flowing through the coil increases, so does the Lorentz force. However, as mentioned above, the maximum current that can be transmitted through the inductive link of the KNUH BCI system is 7.5 mA. The height of the coil that meets this requirement is 2 mm (600 turns, 180 Ω) and the Lorentz force generated is 1,296 mN.

The additional air gap between the coil and metal yoke cylinder allows the coil to vibrate. Therefore, the leakage flux is greater than that of the magnet vibration-type device. To compare the effect on the Lorentz force, the older transducer was also electromagnetically analyzed (Fig. 5), and met the requirement when the coil height was 2 mm; the Lorentz force was 1,353.1 mN at this time. The change in coil vibration reduced the Lorentz force by about 4.2%. However, greater vibration displacement was expected given the reduction in driver mass loading. To confirm this, we performed mechanical vibration analyses.

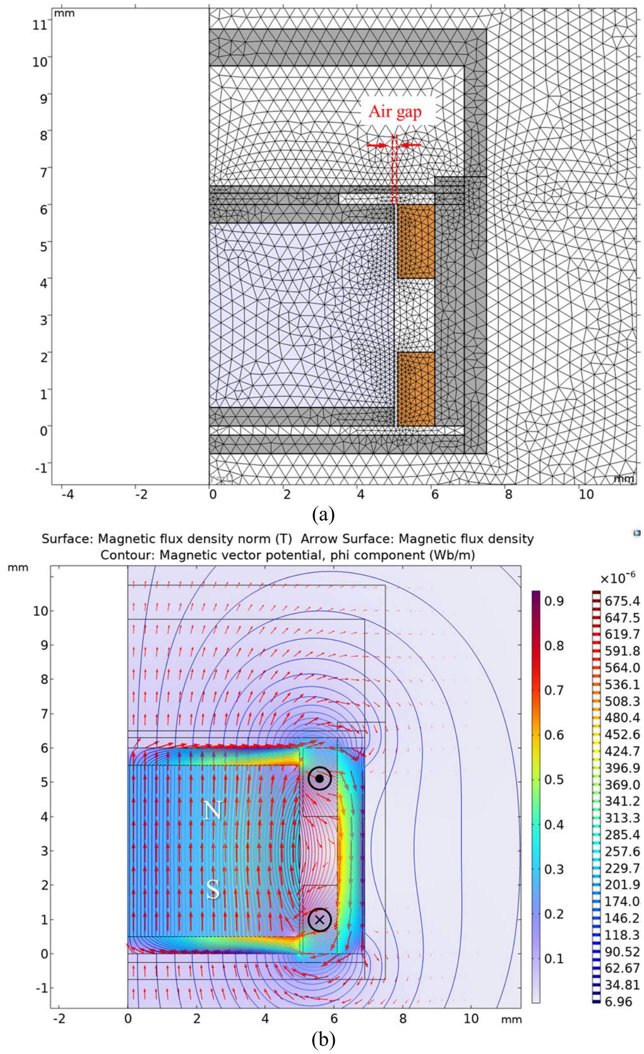

FIGURE 5. (a) Two-dimensional axisymmetric model of the magnet vibration-type BCI transducer and (b) magnetic flux density according to the magnetic flux linkage between the permanent magnet and the coil.

C. MECHANICAL VIBRATIONAL ANALYSIS

We derived the mechanical resonance frequency and vibration displacement of the coil vibration transducer. Most BCI transducers used to treat conductive or mixed-type hearing loss have a mechanical resonance of 0.7–1 kHz [44]. The resonance of the older transducer studied herein is 0.9 kHz [37]. Therefore, we set the mechanical resonance of the coil vibration transducer to 0.9 kHz. To derive the mechanical resonance of the transducer, a vibrational membrane with a diameter of 12.2 mm and four cantilevers was used [Fig. 6(a)]. The location of mechanical resonance was determined based on the spring constant of the vibrational membrane and mass suspended from the membrane. The spring constant is affected by several factors such as membrane width, thickness, and angle, and the number of cantilevers. When setting the mechanical resonance location, it is easier to adjust the membrane spring constant than the mass. To simplify the analysis, only the cantilever angle was changed; the membrane width was fixed at 1 mm and the thickness at 0.2 mm (four cantilevers). The material properties of the vibrational membrane were as follows: Density 7,850 kg/m^3; Poisson's ratio 0.31; and Young's modulus, 205E9 N/m^2. For mechanical vibration analysis, all elements (except the titanium housing and metal yoke cylinder) were created using a 3D mesh model [Fig. 6(b)] with a free tetrahedral comprising 62,567 domain, 21,158 boundary, and 3,244 edge elements (maximum element size = 0.671 mm, minimum size = 0.0488 mm, maximum growth rate = 1.4,

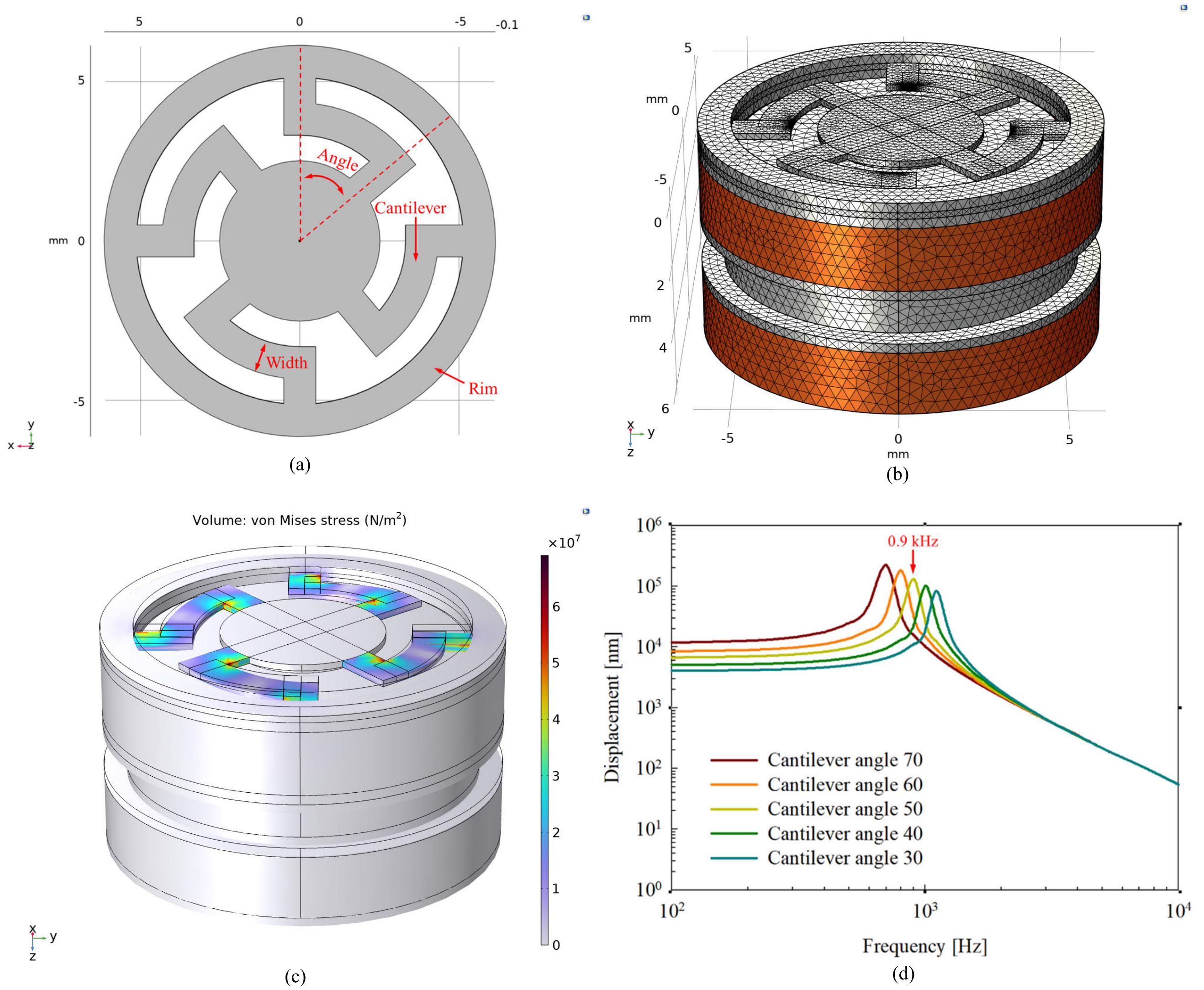

FIGURE 6. **(a) The vibrational membrane composed of four cantilevers; (b) the 3D mesh model of the coil vibration transducer; (c) the maximum distortion energy density distribution map; and (d) the vibration displacements according to the cantilever angle.**

curvature factor = 0.4, narrow region resolution = 0.7). The characteristics of the permanent magnet, metal yoke plate, and circular plate, which are not involved in vibration, were set according to the fixed constraint command values of the solid mechanics routine. The motions of the top and bottom coils, titanium jig, and vibrational membrane moved by the Lorentz force were set to "free/free" using the prescribed displacement command. The total force applied to the coil was 1,296 mN, derived as described above. The total mass loading of the vibrational membrane was 1.114 g (coil = 0.385 g, titanium jig = 0.144 g, metal ring = 0.1 g). To determine the shape of a vibrational membrane with a mechanical resonance (0.9 kHz) appropriate for conductive hearing loss compensation, analysis was performed while changing the angle of the cantilever from 30° to 70° in 10° increments. Fig. 6(c) and (d) show the static data (maximum distortion energy density distribution map at each point under load, i.e., the von Mises stress) and dynamic results (frequency response characteristics according to the cantilever angle). When the angle was 50°, mechanical resonance was generated at 0.9 kHz (as revealed by dynamic analysis) and the critical stress of the vibrational membrane was 6.91E7 N/m^2 (as revealed by static analysis).

The older magnet vibration transducer was subjected to the same analysis. The total force applied to the coil was 1,353.1 mN, derived as described above. Fig. 7(a) shows the von Mises stress of a magnet vibration transducer and the critical stress of the vibrational membrane was 2.47E7 N/m^2. When the cantilever membrane angle was 50°, mechanical resonance was occurred at 0.9 kHz. The membrane specifications were as follows: four cantilevers, diameter of 13.8 mm, width of 0.2 mm, and thickness of 2 mm. The total mass loading was 3.63 g (permanent magnet = 2.974 g, metal yoke plate = 0.328 g). Fig. 7(b) compares the vibrational

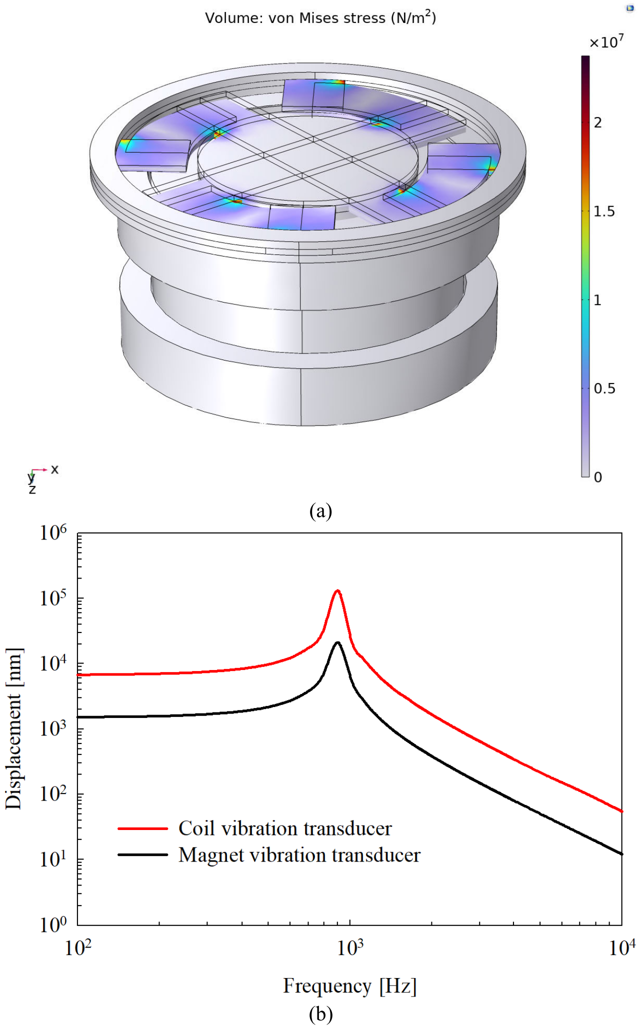

FIGURE 7. (a) Maximum distortion energy density distribution map of the magnet vibration transducer and (b) vibrational displacements of both transducers according to frequency at a driving voltage of 2.7 V_p.

displacements of the two transducers by frequency at the same driving voltage. The coil vibration transducer (1,296 mN) generated about 4.2% less Lorentz force than the older magnet transducer (1,353.1 mN), but the average vibrational displacement was about 4.4-fold higher.

III. IMPLEMENTATION AND MEASUREMENT

A. FABRICATION OF THE NEW TRANSDUCER

Fig. 8 shows the components of the fabricated coil vibration transducer. The vibrational membrane (diameter = 12.2 mm, angle = 50°, thickness = 0.2 mm), circular plate (diameter = 5 mm, thickness = 0.3 mm) and metal ring (outer diameter = 12.2 mm, inner diameter = 10.2 mm, thickness = 0.3 mm) were manufactured by wet etching (a photochemical technique) stainless steel 316L [37]. The titanium housing (Ti-6Al-4V ELI; outer diameter = 15 mm, inner diameter = 13.8 mm, height = 7.5 mm) and cap (Ti-6Al-4V ELI; diameter = 15 mm, height = 4 mm), metal yoke cylinder (Mu-metal; outer diameter = 13.8 mm, inner diameter = 12.4 mm, height = 6 mm), plate (Mu-metal; diameter = 10 mm, height =0.5 mm) and titanium jig (Ti-6Al-4V ELI; outer diameter = 12.2 mm, inner diameter = 10.2 mm, height = 2 mm) were manufactured by CNC machining. The permanent magnet (NdFeB N38AH; Curie temperature = 220°C, diameter = 10 mm, height = 5 mm) was custom-made to ensure that magnetism was not lost when conduction heat was generated during silicon coating. Each coil was automatically wound (600 turns) using self-bonding wire (Solabond PSP15; Elektrisola, Germany) of thickness 0.059 mm and resistance 180 Ω. The components prepared via etching and the CNC process (except the titanium housing cap) were assembled as precisely as possible, using superglue in a probe station with a microscope. We excluded the titanium cap to allow for LDV-assisted measurements of membrane vibration.

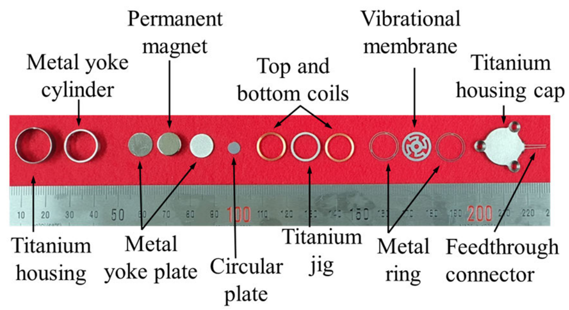

FIGURE 8. Components of the fabricated coil vibration transducer.

B. VIBRATION MEASUREMENT

The vibration displacement characteristics during frequency sweeping (0.1∼10 kHz, 2.7 V_p) of the coil vibration transducer were measured using an LDV system (OFV-5000 vibrometer controller and OFV-534 interferometer sensor head; Polytec GmbH, Waldbronn, Germany) and an automatic data-acquisition system (fast Fourier transform length = 4,096, sampling rate = 96 kHz; average: 10; DAQ, NI PXIe-1071, NI PXIe-8840 and NI PXI-4461; National Instruments Co., Austin, TX, USA); the measurement setup is shown in Fig. 9(a). The acquisition system generates a sinusoidal signal that drives the transducer and stores the vibration signals (displacements) measured by the LDV. To measure only vibration caused by the coil, the titanium housing was firmly fixed to the anti-vibration table using superglue, and the laser beam of the LDV was positioned perpendicular to the rim of the vibrational membrane. The vibration displacement characteristics are shown in Fig. 9(b) according to frequency. The red solid line shows that mechanical resonance was generated at 0.9 kHz, as calculated above (black solid line). However, the vibration after 4 kHz, and the mechanical resonance, differed from the FEA data. The change in mechanical resonance may reflect the fact that we did not consider the viscous damping coefficient or loss factor of the membrane. It is likely that the difference

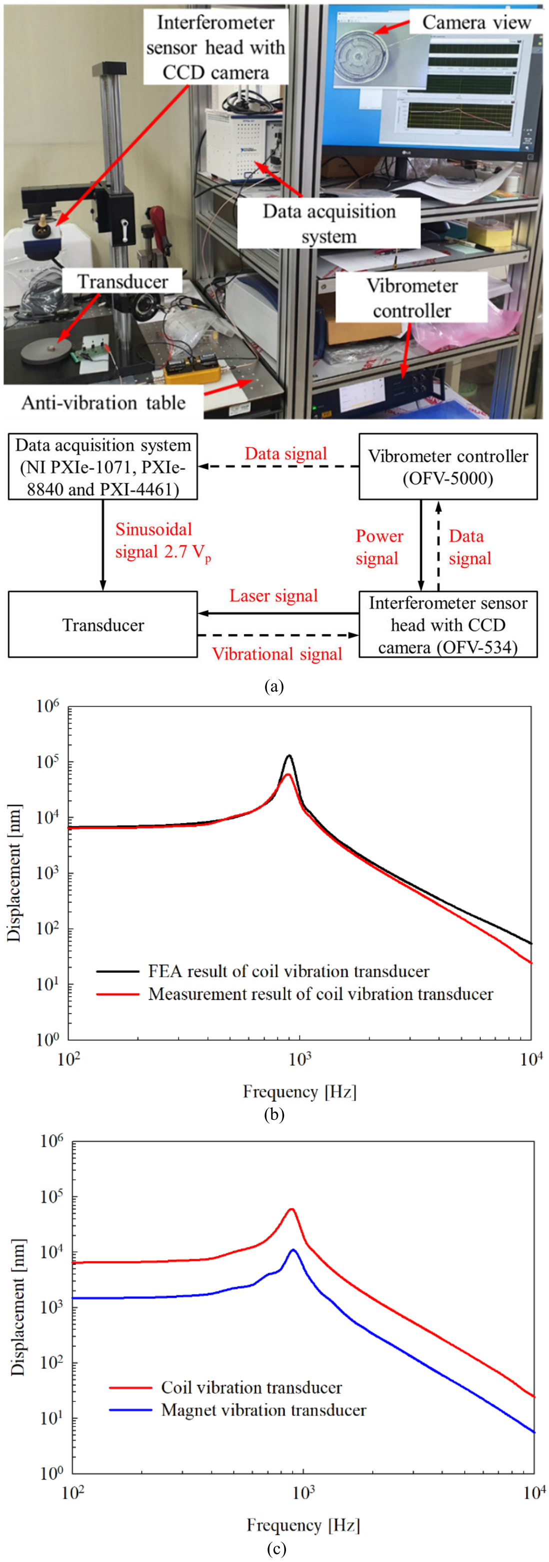

FIGURE 9. **(a) The data acquisition system and block diagram used to measure the transducer vibration characteristics; (b) vibration displacement (measured and FEA data) of the coil vibration transducer and (c) a comparison of the two transducers at the same driving voltage (2.7 V_p).**

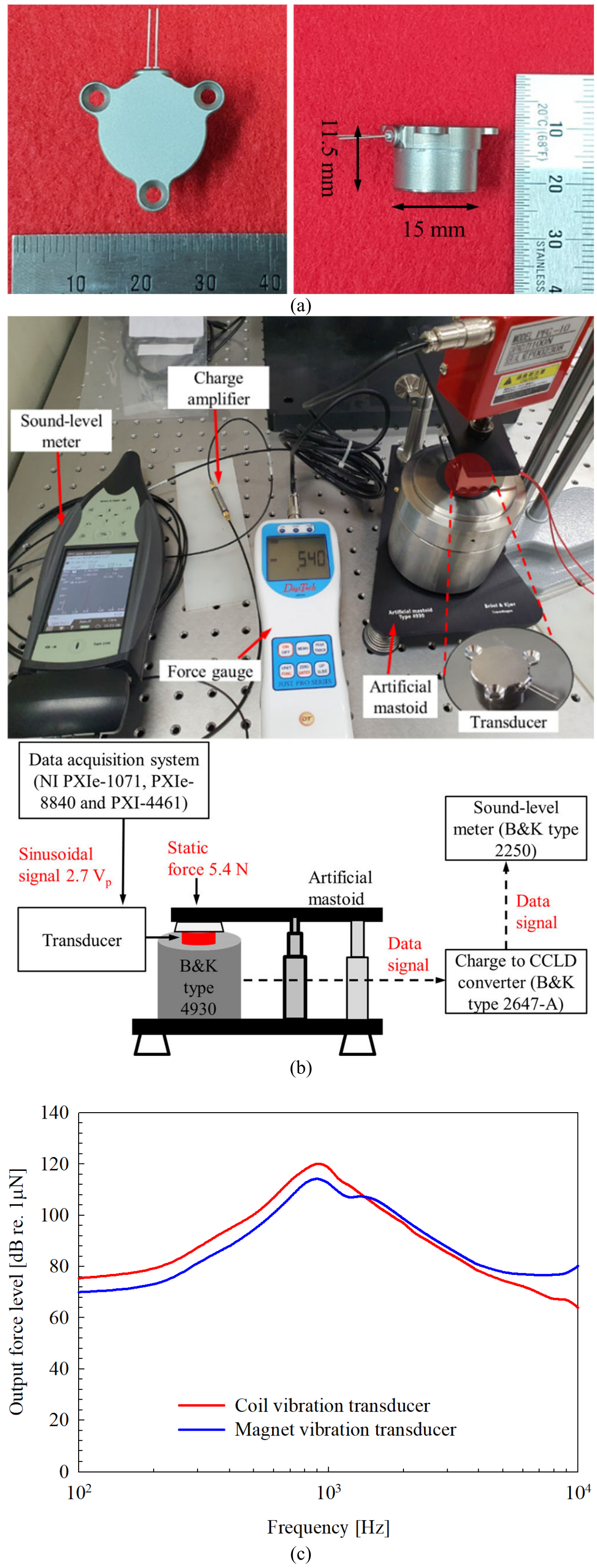

FIGURE 10. **(a) The implemented coil vibration transducer; (b) experimental setup and block diagram used to measure the output force of both transducers using an artificial mastoid; and (c) comparison of the forces.**

in the high-frequency band is attributable to assembly error, such as distortion and misalignment, as we used only superglue. Although the measurement and FEA results thus differed slightly, the general frequency characteristics were as expected, and implementation of the FEA characteristics was successful.

We measured the vibration magnitudes of the two transducers under the same conditions. The vibrations are shown in Fig. 9(c) according to frequency (0.1∼10 kHz); as above, the average vibration of the coil vibration transducer (red solid line, average displacement 6305.1 nm) was about 4.4-fold (∼13 dB) higher than that of the magnet vibration transducer (blue solid line, average displacement 1426.7 nm).

C. EVALUATION OF THE TRANSDUCER OUTPUT

The vibration displacement measurements conducted in this study confirmed that the coil vibration method enhanced the vibration magnitude compared to that of the magnet vibration method under no-load conditions. Thus, the efficiency of the transducer, which consumes most of the BCI power, improved. However, the vibration does not propagate directly to the inner ear, but rather passes through the skull; it was thus important to measure the signal through the skull. We employed an artificial mastoid (type 4930; Brüel & Kjær, Nærum, Denmark) commonly used to measure the forces of bone conduction devices [45], [46], [47], [48]. To this end, the coil vibration transducer was completely assembled including the titanium housing cap [Fig. 10(a)] and placed in the center of the butyl rubber membrane of the artificial mastoid [Fig. 10(b)]. Then, the loading arm was adjusted to the transducer cap surface to apply a static force of 5.4 N, as measured by a force gauge; this met the American National Standard Specification for Audiometers (2010) (ANSI) S3.6 specification [48], [49], [50]. To drive the coil vibration transducer, a sinusoidal signal of 2.7 V_p was applied from 0.1 to 10 kHz and data were acquired automatically. The vibration signals were measured using the artificial mastoid and electrical signals stored in a sound-level meter (type 2250; Brüel & Kjær) after passage through a charge amplifier (type 2647-A; Brüel & Kjær). The magnet vibration transducer was assessed in an identical manner. Fig. 10(c) shows the maximum power output (MPO) of the transducer measured using the artificial mastoid; this is the maximum voltage that can be applied to the transducer in the KNUH BCI system. Below 1.4 kHz, the coil vibration transducer had an output that was 5.5-dB higher on average. However, at 1.4–4 kHz and > 4 kHz, the magnet vibration transducer had average outputs that were 1.9 dB and 7.6 dB higher, respectively, compared with the coil vibration transducer. The vibration measurement data in Fig. 9(c) show that the average vibration of the coil vibration transducer was 13 dB higher at all frequency bands. The experimental results differed. Fig. 10(c) shows that the coil vibration transducer had a higher output force only below 1.4 kHz. This may be attributable to the use of a mass about 3.25-fold lighter than that of the driver of the magnet vibration transducer. Thus, when the mass of the driver is low, vibration transmission is attenuated as the frequency increases. Our results emphasize that bone conduction transducers should be evaluated using a calibration device, such as an artificial mastoid, rather than under no-load conditions. Although the output force in the high-frequency region was lower than that of the older transducer, the improvement was about 2 dB in the speech frequency region, i.e., the region critical for speech intelligibility and perception (up to 3 kHz). Therefore, our device will aid the hearing-impaired.

IV. CONCLUSION

We developed a coil vibration BCI transducer; vibration displacement was improved by reducing the mass loading of the transducer driver. Electromagnetic and mechanical vibration analyses were performed to derive the maximum Lorentz force of the transducer and optimal frequency for conductive hearing loss compensation. The data were compared to those of the magnet vibration transducer. Under the same driving voltage (2.7 V_p) and mechanical resonance (0.9 kHz), the Lorentz force of the coil vibration transducer was about 4.2% lower than that of the magnet vibration transducer, while the vibration magnitude was about 4.4-fold (13 dB) higher. Both transducers were fabricated and the frequency characteristics were measured using an LDV and data acquisition system. The displacement amplitude of the coil vibration transducer was about 4.4-fold higher than that of the magnet vibration transducer, in line with the FEA results. The output force of both transducers was measured using an artificial mastoid. The coil vibration transducer had higher output only below 1.4 kHz; the output force of the coil vibration transducer tended to be lower than that of the magnet vibration transducer at high frequencies. These results emphasize that transducer performance should be assessed by deriving output forces using a calibration device (such as an artificial mastoid) rather than by measuring membrane vibration under no-load conditions. As bone conduction hearing aids are indicated for conductive hearing loss (poor low-frequency hearing), the new transducer will function better than the older one. Future optimization of driver mass loading will improve the output power at all frequencies.

We bench tested the transducer using an artificial mastoid, which is commonly employed to measure the force of a bone conduction device. However, because artificial mastoid does not reflect on actual bone density of human, the derived measurements by using artificial mastoid might differ from those obtained by using human bone implant. Therefore, to predict actual effects more than bench test did in implantable medical devices, preclinical studies are required, and we plan cadaveric and animal experiments.

REFERENCES

[1] C. Schmucker, P. Kapp, E. Motschall, J. Loehler, and J. J. Meerpohl, ''Prevalence of hearing loss and use of hearing aids among children and adolescents in Germany: A systematic review,'' *BMC Public Health*, vol. 19, no. 1, pp. 1–10, Sep. 2019.

[2] J. Besser, M. Stropahl, E. Urry, and S. Launer, ''Comorbidities of hearing loss and the implications of multimorbidity for audiological care,'' *Hearing Res.*, vol. 369, pp. 3–14, Nov. 2018.

[3] B. O. Olusanya, A. C. Davis, and H. J. Hoffman, ''Hearing loss grades and the international classification of functioning, disability and health,'' *Bull. World Health Org.*, vol. 97, no. 10, pp. 725–728, Oct. 2019.

[4] R. L. Goode, M. L. Rosenbaum, and A. J. Maniglia, "The history and development of the implantable hearing AID," *Otolaryngol. Clinics North Amer.*, vol. 28, no. 1, pp. 1–16, Feb. 1995.

[5] D. S. Haynes, J. A. Young, G. B. Wanna, and M. E. Glasscock, "Middle ear implantable hearing devices: An overview," *Trends Amplification*, vol. 13, no. 3, pp. 206–214, 2009.

[6] H. H. Kim and D. M. Barrs, "Hearing aids: A review of what's new," *Otolaryngol. Head Neck Surg.*, vol. 134, no. 6, pp. 1043–1050, Jun. 2006.

[7] D. H. Shin and J.-H. Cho, "Design and development of a tri-coil bellows transducer for RW-drive implantable middle-ear hearing aid using FEA," *IEEE/ASME Trans. Mechatronics*, vol. 23, no. 3, pp. 1436–1444, Jun. 2018.

[8] H. A. Jenkins, J. S. Atkins, D. Horlbeck, M. E. Hoffer, B. Balough, G. Alexiades, and W. Garvis, "Otologics fully implantable hearing system: Phase I trial 1-year results," *Otol. Neurotol.*, vol. 29, no. 4, pp. 534–541, Jun. 2008.

[9] V. Colletti, M. Carner, and L. Colletti, "TORP vs round window implant for hearing restoration of patients with extensive ossicular chain defect," *Acta Oto-Laryngol.*, vol. 129, no. 4, pp. 449–452, Jan. 2009.

[10] J. B. Firszt, L. K. Holden, R. M. Reeder, L. Cowdrey, and S. King, "Cochlear implantation in adults with asymmetric hearing loss," *Ear Hearing*, vol. 33, no. 4, pp. 521–533, Jul. 2012.

[11] D. H. Shin, K. W. Seong, H. H. Nakajima, S. Puria, and J.-H. Cho, "A piezoelectric bellows round-window driver (PBRD) for middle-ear implants," *IEEE Access*, vol. 8, pp. 137947–137954, 2020.

[12] B. Håkansson, S. Reinfeldt, M. Eeg-Olofsson, P. Östli, H. Taghavi, J. Adler, J. Gabrielsson, S. Stenfelt, and G. Granström, "A novel bone conduction implant (BCI): Engineering aspects and pre-clinical studies," *Int. J. Audiol.*, vol. 49, no. 3, pp. 203–215, Jan. 2010.

[13] A. Mudry and L. Dodelé, "History of the technological development of air conduction hearing aids," *J. Laryngol. Otol.*, vol. 114, no. 6, pp. 418–423, Jun. 2000.

[14] U. Fisch, W. R. J. Cremers, T. Lenarz, B. Weber, G. Babighian, A. S. Uziel, D. W. Proops, A. F. O'Connor, R. Charachon, J. Helms, and B. Fraysse, "Clinical experience with the vibrant soundbridge implant device," *Otol. Neurotol.*, vol. 22, no. 6, pp. 962–972, Nov. 2001.

[15] A. Dhanasingh and C. Jolly, "An overview of cochlear implant electrode array designs," *Hearing Res.*, vol. 356, pp. 93–103, Dec. 2017.

[16] D. W. Maidment, A. B. Barker, J. Xia, and M. A. Ferguson, "A systematic review and meta-analysis assessing the effectiveness of alternative listening devices to conventional hearing aids in adults with hearing loss," *Int. J. Audiol.*, vol. 57, no. 10, pp. 721–729, Oct. 2018.

[17] H. Amieva and C. Ouvrard, "Does treating hearing loss in older adults improve cognitive outcomes? A review," *J. Clin. Med.*, vol. 9, no. 3, p. 805, Mar. 2020.

[18] P. Burke, I. Jardim, R. Brito, R. Tsuji, A. Fonseca, R. Bento, and A. Bittencourt, "Implantable and semi-implantable hearing aids: A review of history, indications, and surgery," *Int. Arch. Otorhinolaryngol.*, vol. 18, no. 3, pp. 303–310, Apr. 2014.

[19] A. Winkler, M. Latzel, and I. Holube, "Open versus closed hearing-aid fittings: A literature review of both fitting approaches," *Trends Hearing*, vol. 20, Feb. 2016, Art. no. 233121651663174.

[20] I. Mosnier, O. Sterkers, D. Bouccara, and S. Labassi, "Benefit of the vibrant soundbridge device in patients implanted for 5 to 8 years," *Ear Hearing*, vol. 29, no. 2, pp. 281–284, Apr. 2008.

[21] S. Labassi, M. Beliaeff, V. Péan, and P. V. Heyning, "The vibrant soundbridge middle ear implant: A historical overview," *Cochlear Implants Int.*, vol. 18, no. 6, pp. 314–323, Aug. 2017.

[22] P. P. Lefebvre, C. Martin, C. Dubreuil, M. Decat, A. Yazbeck, J. Kasic, and S. Tringali, "A pilot study of the safety and performance of the otologics fully implantable hearing device: Transducing sounds via the round window membrane to the inner ear," *Audiol. Neurotol.*, vol. 14, no. 3, pp. 172–180, 2009.

[23] G. A. Channer, A. A. Eshraghi, and L. X. Zhong, "Middle ear implants: Historical and futuristic perspective," *J. Otol.*, vol. 6, no. 2, pp. 10–18, Dec. 2011.

[24] E. Glennon, M. A. Svirsky, and R. C. Froemke, "Auditory cortical plasticity in cochlear implant users," *Current Opinion Neurobiol.*, vol. 60, pp. 108–114, Feb. 2020.

[25] F.-G. Zeng, S. Rebscher, W. V. Harrison, X. Sun, and H. Feng, "Cochlear implants: System design, integration, and evaluation," *IEEE Rev. Biomed. Eng.*, vol. 1, pp. 115–142, 2008.

[26] R. Weiss, A. Loth, M. Leinung, S. Balster, D. Hirth, T. Stöver, S. Helbig, and S. Kramer, "A new adhesive bone conduction hearing system as a treatment option for transient hearing loss after middle ear surgery," *Eur. Arch. Oto-Rhino-Laryngol.*, vol. 277, no. 3, pp. 751–759, Mar. 2020.

[27] A. Canale, V. Boggio, A. Albera, M. Ravera, F. Caranzano, M. Lacilla, and R. Albera, "A new bone conduction hearing aid to predict hearing outcome with an active implanted device," *Eur. Arch. Oto-Rhino-Laryngol.*, vol. 276, no. 8, pp. 2165–2170, May 2019.

[28] A. Magele, P. Schoerg, B. Stanek, B. Gradl, and G. M. Sprinzl, "Active transcutaneous bone conduction hearing implants: Systematic review and meta-analysis," *PLoS ONE*, vol. 14, no. 9, Sep. 2019, Art. no. e0221484.

[29] S. Reinfeldt, B. Håkansson, H. Taghavi, and M. Eeg-Olofsson, "New developments in bone-conduction hearing implants: A review," *Med. Devices: Evidence Res.*, vol. 8, pp. 79–93, Jan. 2015.

[30] D. C. P. B. M. van Barneveld, H. J. W. Kok, J. F. P. Noten, A. J. Bosman, and A. F. M. Snik, "Determining fitting ranges of various bone conduction hearing aids," *Clin. Otolaryngol.*, vol. 43, no. 1, pp. 68–75, Feb. 2018.

[31] A. Sarasty and M. Zernotti, "Active bone conduction prosthesis: BonebridgeTM," *Int. Arch. Otorhinolaryngol.*, vol. 19, no. 4, pp. 343–348, Oct. 2015.

[32] M. Manrique, I. Sanhueza, R. Manrique, and J. de Abajo, "A new bone conduction implant: Surgical technique and results," *Otol. Neurotol.*, vol. 35, no. 2, pp. 216–220, Feb. 2014.

[33] S. K. Plontke, G. Götze, C. Wenzel, T. Rahne, and R. Mlynski, "Implantation of a new active bone conduction hearing device with optimized geometry," *HNO*, vol. 68, no. S2, pp. 106–115, Aug. 2020.

[34] G. Mertens, J. Desmet, A. F. Snik, and P. Van de Heyning, "An experimental objective method to determine maximum output and dynamic range of an active bone conduction implant: The Bonebridge," *Otol. Neurotol.*, vol. 35, no. 7, pp. 1126–1130, Aug. 2014.

[35] J. J. Eggermont, *Hearing Loss: Causes, Prevention, and Treatment*. Cambridge, MA, USA: Academic, 2017.

[36] D. H. Shin, K. W. Seong, E. S. Jung, J.-H. Cho, and K.-Y. Lee, "Design of a dual-coil type electromagnetic actuator for implantable bone conduction hearing devices," *Technol. Health Care*, vol. 27, pp. 445–454, Jun. 2019.

[37] S. H. Lee, K. W. Seong, K.-Y. Lee, and D. H. Shin, "Optimization and performance evaluation of a transducer for bone conduction implants," *IEEE Access*, vol. 8, pp. 100448–100457, 2020.

[38] S. Stenfelt, "Acoustic and physiologic aspects of bone conduction hearing," *Adv. Oto-Rhino-Laryngol.*, vol. 71, no. 2, pp. 10–21, Mar. 2012.

[39] S. E. Ellsperman, E. M. Nairn, and E. Z. Stucken, "Review of bone conduction hearing devices," *Audiol. Res.*, vol. 11, no. 2, pp. 207–219, May 2021.

[40] M. K. S. Hol, R. C. Nelissen, M. J. H. Agterberg, C. W. R. J. Cremers, and A. F. M. Snik, "Comparison between a new implantable transcutaneous bone conductor and percutaneous bone-conduction hearing implant," *Otol. Neurotol.*, vol. 34, no. 6, pp. 1071–1075, Aug. 2013.

[41] S. Stenfelt, "Transcranial attenuation of bone-conducted sound when stimulation is at the mastoid and at the bone conduction hearing aid position," *Otol. Neurotol.*, vol. 33, no. 2, pp. 105–114, Feb. 2012.

[42] B. Balachandran and E. B. Magrab, *Vibrations*. Cambridge, U.K.: Cambridge Univ. Press, 2018.

[43] S. S. Rao and F. F. Yap, *Mechanical Vibrations*. Boston, MA, USA: Addison-Wesley, 1995.

[44] H. Taghavi, B. Håkansson, and S. Reinfeldt, "A novel bone conduction implant-analog radio frequency data and power link design," in *Proc. 9th IASTED Int. Conf. Biomed. Eng.*, Innsbruck, Austria, 2012, pp. 327–335.

[45] S. Surendran and S. Stenfelt, "The outer ear pathway during hearing by bone conduction," *Hearing Res.*, vol. 421, Aug. 2022, Art. no. 108388.

[46] B. Håkansson, K.-J. Fredén Jansson, T. Tengstrand, L. Johannsen, M. Eeg-Olofsson, C. Rigato, E. Dahlström, and S. Reinfeldt, "VEMP using a new low-frequency bone conduction transducer," *Med. Devices: Evidence Res.*, vol. 11, pp. 301–312, Sep. 2018.

[47] B. Håkansson, F. Woelflin, A. Tjellström, and W. Hodgetts, "The mechanical impedance of the human skull via direct bone conduction implants," *Med. Devices: Evidence Res.*, vol. 13, pp. 293–313, Sep. 2020.

[48] M. Ghoncheh, T. Lenarz, and H. Maier, "A precision driver device for intraoperative stimulation of a bone conduction implant," *Sci. Rep.*, vol. 10, no. 1, p. 1797, Feb. 2020.

[49] R. H. Margolis and S. M. Stiepan, "Acoustic method for calibration of audiometric bone vibrators," *J. Acoust. Soc. Amer.*, vol. 131, no. 2, pp. 1221–1225, Feb. 2012.

[50] K. A. Pollard, P. K. Tran, and T. R. Letowski, "A free-field method to calibrate bone conduction transducers," *J. Acoust. Soc. Amer.*, vol. 133, no. 2, pp. 858–865, Feb. 2013.

KI WOONG SEONG received the B.S., M.S., and Ph.D. degrees in electronics engineering from Kyungpook National University, Daegu, South Korea, in 1998, 2000, and 2010, respectively.

From 2010 to 2011, he was a Research Professor at the Institute of Biomedical Engineering Research, Kyungpook National University. Since 2012, he has been a Professor with the Department of Biomedical Engineering, Kyungpook National University Hospital, South Korea. His research interests include implantable hearing aids, bioelectronics, biomedical signal processing, and sensor applications in biomedical instrumentations.

DONG HO SHIN received the B.S. degree in electronics engineering from Dongseo University, Busan, South Korea, in 2009, and the M.S. and Ph.D. degrees from the School of Electronics Engineering, Kyungpook National University, South Korea, in 2011 and 2016, respectively.

From 2016 to 2019, he was a Research Fellow at the Institute of Biomedical Engineering Research, Kyungpook National University, where he is currently a Research Professor. His research interests include electronic and mechanical system of medical instruments and middle-ear implants transducer.

KYU-YUP LEE received the B.S., M.S., and Ph.D. degrees from the School of Medicine, Kyungpook National University, Daegu, South Korea, in 1996, 2003, and 2008, respectively.

Since 2004, he has been a Professor with the Department of Otorhinolaryngology-Head and Neck Surgery, School of Medicine, Kyungpook National University. His research interests include hearing rehabilitation device, ear and mastoid disease, implantable bone conduction hearing aids, and sensor applications in biomedical instrumentations.